SESSION 3. FINITE ELEMENTS

Session Chairman

R. H. Mallett*

Bell Aerospace Corp.
Buffalo, New York

*now with Westinghouse Electric Corp., Madison, Pa.

COMPARISON OF TWO HIGH-PRECISION TRIANGULAR FINITE ELEMENTS FOR ARBITRARY DEEP SHELLS

by

G. Richard Cowper* and Garry M. Lindberg**
National Aeronautical Establishment
National Research Council of Canada

and

Mervyn D. Olson***
Department of Civil Engineering,
University of British Columbia.

Two approaches to the finite element analysis of arbitrary deep shells are presented and compared. One approach involves the derivation of a suitable transformation to link shallow shell elements together to form deep shells. The second approach involves the derivation of a curvilinear element based on the general tensorial formula for the strain energy of a thin shell. Both approaches use higher order interpolation functions and both result in triangular finite elements with 36 degrees of freedom, 12 at each node. Results confirm that both approaches give accurate predictions of stresses as well as displacements. Solutions rapidly converge as the number of elements is increased and engineering accuracy is always attained with just a few elements.

1.0 INTRODUCTION

The finite element analysis of shells has been studied extensively during the past decade. An extensive critical survey of developments up to 1969 has been given by Gallagher [1], while more limited surveys have been given by Zienkiewicz [2], Key [3], Hartung [4], and by the authors [5]. It is fair to say that no one element has won general acceptance, and also that many of the available elements impose limitations on the shape of the shell, for example, the limitation to shells of revolution.

During the past few years the authors have developed a number of triangular high-precision finite elements for plate bending [6,7], plane stress [8], shallow shells [8] and cylindrical shells [9]. These elements use higher order interpolation polynomials and result in smaller overall problem size, give accurate predictions of stresses, and satisfy sufficient conditions to guarantee rapid convergence to the exact solutions. This family is now enlarged to permit the analysis of deep shells of general shape.

---

*Senior Research Officer; **Associate Research Officer; ***Assistant Professor.

Two approaches are presented. The first is derivation of a curvilinear triangular element based on the general tensorial formula for the strain energy of a thin shell. The second is the derivation of a suitable transformation to link shallow shell elements together to form deep shells. Although the first approach was expected to yield better results, the second approach promised some advantages such as the avoidance of numerical integration and of the complexities of tensor notation. Moreover, available computer routines for shallow shells could be exploited in the second approach. Following a description of the two approaches, the derived elements are tested on certain problems and their performance is compared.

2.0 THE GENERAL SHELL ELEMENT (CURSHL)

The following derivation is very brief but complete details are available [10]. Let α,β be curvilinear coordinates on the shell surface, not necessarily orthogonal nor principal. The same displacement functions which have been used successfully in earlier high-precision elements are also adopted for the general shell element. The normal displacement w is taken as a restricted quintic polynomial in the coordinates α,β, while the tangential displacements u, v are taken as complete cubic polynomials in α,β. In keeping with the assumed displacement functions, the generalized displacements are the values of u, $\partial u/\partial\alpha$, $\partial u/\partial\beta$, v, $\partial v/\partial\alpha$, $\partial v/\partial\beta$, w, $\partial w/\partial\alpha$, $\partial w/\partial\beta$, $\partial^2 w/\partial\alpha^2$, $\partial^2 w/\partial\alpha\partial\beta$, $\partial^2 w/\partial\beta^2$ at the three vertices of the element, a total of 36 degrees of freedom per element. Centroidal displacements u_c, v_c, are used during the development of the stiffness matrix but are later eliminated by static condensation.

The choice of displacement functions and generalized displacements assures that u, v, w, and first derivatives of w are continuous between elements. Conformity, however, requires that the displacement vector and the rotations of the normal be continuous. If the shell is smooth, continuity of the displacement vector is equivalent to continuity of the components u, v, w. In general shell theories, the formulas for rotations involve the first derivatives of w plus products of u, v with the shell curvature. Therefore continuity of u, v, w, and first derivatives of w implies continuity of rotations, provided that the shell curvature is continuous. In Donnell-Vlasov theory and in shallow shell theory the rotations are approximated by the first derivatives of w. In these cases, continuity of rotations is equivalent to continuity of the first derivatives of w regardless of the continuity of shell curvatures.

The highest derivatives of displacement which appear in the expression for strain energy are the second derivatives of w and first derivatives of u, v. Since the interpolation function for w contains a complete quartic polynomial, it follows from Taylor's theorem that the finite element can represent any distribution of second derivatives of w with an error of order h^3, where h is a typical linear dimension of the element. Likewise, the first derivatives of u, v, are represented with an error of order h^3,

since the interpolation functions for u, v are complete cubic polynomials. Then, according to the theorem of minimum potential energy [11,6] the element should have a discretization error in the strain energy of order h^6.

Some authorities [1,12,13] advocate the use of equal order polynomials for the displacements u, v, w. This is not necessary for conformity nor is it efficient. Using quintic polynomials for all of u, v, w, would result in only marginal improvements in accuracy because the order of the error in the strain energy would still be limited by the accuracy of w. Moreover, this marginal improvement would be bought at the price of a 50% increase in the degrees of freedom, from 12 per node to 18 per node. On the other hand, the use of equal order polynomials for u, v, w, facilitates the handling of non-smooth junctions of shells.

Little consideration has been given to obtaining exact rigid-body modes, a point which has often been over-emphasized. Rather, the focus of attention has been the error in the strain energy. Making the error in strain energy acceptably small automatically ensures that rigid-body motions are adequately represented.

Lack of space precludes more than a sketch of the computational procedure. Let {W} be the vector of nodal displacements of an element and let {F(α,β)} be the vector of displacements and their derivatives at a general point α,β, within the element, thus

$$\{F\}^T = \{u,\ u_\alpha,\ u_\beta,\ v,\ v_\alpha,\ v_\beta,\ w,\ w_\alpha,\ w_\beta,\ w_{\alpha\alpha},\ w_{\alpha\beta},\ w_{\beta\beta}\} \quad (1)$$

where the subscripts on u, v, w, denote derivatives. The vector {F} can be related to {W}, thus

$$\{F\} = [S]\{W\} \quad (2)$$

where [S] is a matrix of interpolation polynomials. Let {e} be the vector of membrane and bending strains,

$$\{e\}^T = \{\varepsilon_{11},\ \varepsilon_{12},\ \varepsilon_{22},\ \kappa_{11},\ \kappa_{12},\ \kappa_{22}\} \quad (3)$$

and let {e} be related to {F} by

$$\{e\} = [B]\{F\} \quad (4)$$

The form of [B] depends on which shell theory is used. The computer program which has been developed allows the options of using either Koiter-Sanders theory [14,15], Donnell-Vlasov theory [16] or shallow shell theory [16,17]. In all three cases continuous Kirchoff constraints are applied.

The strain energy of the element can be written

$$U_e = \tfrac{1}{2}\int\int \{e\}^T[E]\{e\}\sqrt{a}\ d\alpha d\beta \quad (5)$$

where [E] is the matrix of bending and stretching rigidities and a is the determinant of the metric tensor. The matrix [E], which

is the same for each of the above three shell theories, is limited in the program to isotropic materials, but variable thickness can be accommodated. It follows from (2), (4), and (5) that

$$U_e = \tfrac{1}{2}\{W\}^T(\int\int[S]^T[B]^T[E][B][S]\sqrt{a}\ d\alpha d\beta)\{W\} \qquad (6)$$

and hence the stiffness matrix is given by

$$[K] = \int\int[S]^T[B]^T[E][B][S]\sqrt{a}\ d\alpha d\beta \qquad (7)$$

For the sake of generality the tensorial form of shell theory was used in setting up the matrices [B] and [E]. The quantities u, v, w, therefore are tensor components of displacement, in contrast to the physical components which are used in other high-precision elements. Computer output routines, which convert tensor components to physical components, have been developed.

Because of the complexity of formula (7) and because so many of the terms of matrices [B] and [E] may be variables, it was decided to abandon the closed-form integration which has been used in previous high-precision elements and to use numerical integration instead to evaluate (7). A newly-developed 13-point numerical integration formula, which has an error of order h^8, is used [10]. A numerical integration formula with error of order h^8 was selected to retain the energy-bounding property of conforming elements. For conforming finite elements of the displacement type the discretization error in strain energy is known to be negative. Since the discretization error of the element is of order h^6, the error of numerical integration should be small compared with the discretization error and the total error in strain energy should still be negative. Hence the calculated strain energy should still be a lower bound on the true strain energy. As will be seen later the attempt to retain the energy-bounding property has not been entirely successful.

The matrix [B] involves many geometric quantities dependent on the shape of the shell, such as metric and curvature tensors and Christoffel symbols. The values of these quantities at the pivotal points of the integration formula must be known in order to evaluate (7). It is assumed that the shell surface is defined by the equations

$$x = x(\alpha,\beta), \qquad y = y(\alpha,\beta), \qquad z = z(\alpha,\beta) \qquad (8)$$

where x, y, z are Cartesian coordinates of a general point on the shell. The required geometric quantities can be computed from x, y, z and their derivatives using standard formulae [18]. Derivatives up to third order are required in Koiter-Sander's theory while second order derivatives of x, y, z suffice in Donnell-Vlasov and shallow shell theory. This data is fed into the computer program from a user-supplied subroutine which must return the values of x, y, z and their derivatives at any arbitrarily given point α,β. If, as is generally the case, the shell surface is of simple form then the exact equations of the surface can be used in setting up the subroutine. On the other hand, the representation of the shell by a fitted polynomial surface is not precluded. In all applications

to date the exact equations of the surface have been used.

The computation of consistent load vectors is similar to the computation of the stiffness matrix. The computer program can accommodate thermal loads as well as arbitrarily distributed body forces on the shell surface. Data on the loads is fed into the program from a second user-supplied subroutine which must return the values of all components of load at an arbitrarily given point α,β.

3.0 THE TRANSFORMED SHALLOW SHELL ELEMENT (TSS)

The following derivations are necessarily brief, but full details are available in Ref. 19. This work is a natural extension of the simplified transformation proposed in Ref. 5. The main requirement for applying shallow shell elements to an arbitrary deep shell is a suitable transformation between the shallow shell degrees of freedom and those for the deep shell. The shallow shell element of Ref. 8 is used here because it proved to be superior both in ease of formulation and in accuracy to most other shallow shell elements. Further, it leads to the same deep shell degrees of freedom as for the general shell element (Sec. 2) and hence is directly comparable with it.

The relevant geometry is shown in Figure 1, where x, y, z are Cartesian global coordinates, ξ, η, ζ, are Cartesian local coordinates, and α,β are curvilinear shell coordinates lying in the mid-surface of the shell. At this point, the latter need not be orthogonal. The ξ, η coordinates are to be used as the base plane coordinates in the shallow shell formulation and the ξ, η axes are defined to go through the element corner nodes 1, 2, 3 as shown.

Again it is assumed that the shell surface is defined by equations (8) and that derivatives of x, y, z up to second order are available. This leads to a natural computation process in which the element corner nodes are located first by specifying their shell coordinates (α,β), and then their global coordinates (x, y, z) are calculated from equations (8). The element geometry may then be determined from these latter coordinates.

Some results from analytical geometry follow. The global coordinates of the ξ, η, ζ, system origin are

$$\begin{aligned} x_o &= (1-\rho)x_1 + \rho x_2 \\ y_o &= (1-\rho)y_1 + \rho y_2 \\ z_o &= (1-\rho)z_1 + \rho z_2 \end{aligned} \tag{9}$$

where the parameter ρ is

$$\rho = \frac{(x_3-x_1)(x_2-x_1) + (y_3-y_1)(y_2-y_1) + (z_3-z_1)(z_2-z_1)}{(x_2-x_1)^2 + (y_2-y_1)^2 + (z_2-z_1)^2} \tag{10}$$

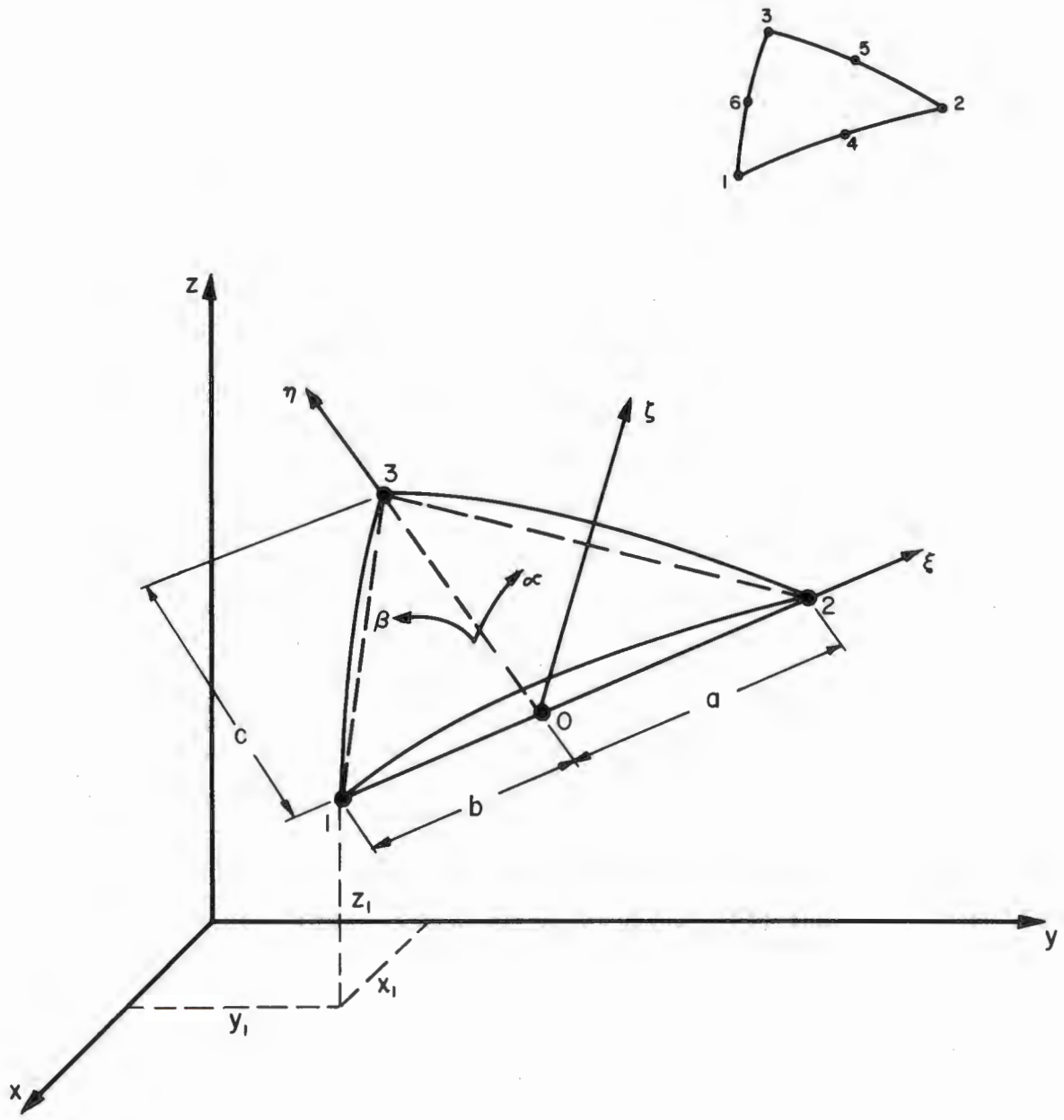

Figure 1. Geometry and Co-Ordinate Systems For Transformed Shallow Shell Formulation

The subscripts denote the element corner nodes 1, 2, 3 of Figure 1. The element dimensions a, b, c are then given by

$$a = (1-\rho)\sqrt{(x_2-x_1)^2 + (y_2-y_1)^2 + (z_2-z_1)^2}$$

$$b = \rho\sqrt{(x_2-x_1)^2 + (y_2-y_1)^2 + (z_2-z_1)^2} \qquad (11)$$

$$c = \sqrt{(x_3-x_0)^2 + (y_3-y_0)^2 + (z_3-z_0)^2}$$

The following relations between the global and local Cartesian coordinates are obtained

$$\xi = [(x_2-x_1)(x-x_0) + (y_2-y_1)(y-y_0) + (z_2-z_1)(z-z_0)]/(a+b)$$

$$\eta = [(x_3-x_0)(x-x_0) + (y_3-y_0)(y-y_0) + (z_3-z_0)(z-z_0)]/c \qquad (12)$$

$$\zeta = b_1\,(x-x_0) + b_2\,(y-y_0) + b_3\,(z-z_0)$$

where

$$b_1 = [(y_2-y_1)(z_3-z_0) - (z_2-z_1)(y_3-y_0)]/(a+b)c$$

$$b_2 = [(z_2-z_1)(x_3-x_0) - (x_2-x_1)(z_3-z_0)]/(a+b)c \qquad (13)$$

$$b_3 = [(x_2-x_1)(y_3-y_0) - (y_2-y_1)(x_3-x_0)]/(a+b)c$$

Combining equations (8) and (12) then yields the base plane coordinates as explicit functions of the shell coordinates, written symbolically as

$$\xi = \xi\,(\alpha,\beta)$$
$$\eta = \eta\,(\alpha,\beta) \qquad (14)$$

Now all the derivatives required in transforming the generalized displacements from local coordinates to shell coordinates may be derived from the above equations.

3.1 Transformation Matrices

The shallow shell formulation of Ref. 8 begins with generalized displacements written relative to the base plane coordinates, w, w_ξ, w_η, etc., and these are now transformed to deep shell ones. The displacement normal to the shell w is a scalar and hence, using equations (14), its derivatives transform simply as

$$(w,\ w_\alpha,\ w_\beta,\ w_{\alpha\alpha},\ w_{\alpha\beta},\ w_{\beta\beta})^T = [R_2](w,\ w_\xi,\ w_\eta,\ w_{\xi\xi},\ w_{\xi\eta},\ w_{\eta\eta})^T \qquad (15)$$

where $[R_2]$ is given in Table 1. The tangential displacements u, v are defined to be parallel to the coordinate axes and hence must be transformed as vectors. Again using results from analytical geometry and the element's shallowness leads to the approximation

$$(u,\ u_\xi,\ u_\eta,\ v,\ v_\xi,\ v_\eta)^T = [R_1](\tilde{u},\ \tilde{u}_\alpha,\ \tilde{u}_\beta,\ \tilde{v},\ \tilde{v}_\alpha,\ \tilde{v}_\beta)^T \quad (16)$$

where $\tilde{u}$ and $\tilde{v}$ are in the directions of α and β, and $[R_1]$ is given in Table 1. Combining all these results and dropping the "tilda" notation for simplicity, the complete transformation for one element is

$$\{W_1\} = [R]\{W_2\} \quad (17)$$

where

$$\{W_2\}^T = (u_1,\ u_{\alpha 1},\ u_{\beta 1},\ v_1,\ v_{\alpha 1},\ v_{\beta 1},\ w_1,\ w_{\alpha 1},\ w_{\beta 1},\ w_{\alpha\alpha 1},\ w_{\alpha\beta 1},\ w_{\beta\beta 1},\ u_2,\ldots\ldots,\ u_3,\ldots\ldots,\ u_c,\ v_c) \quad (18)$$

is the generalized displacement vector in shell coordinates and $[R]$ is the new "rotation" matrix given in Table 1. The 38 × 38 stiffness matrix relative to shell coordinates is then

$$[K] = [R]^T\,[T_1]^T\,[k]\,[T_1]\,[R] \quad (19)$$

where $[T_1]$, $[k]$, $\{W_1\}$, the consistent load vector and the stiffness matrix condensation procedure are the same as in Ref. 8.

It may be seen that the foregoing transformation breaks down if the Jacobian of equations (14) vanishes. This occurs for example at the pole of a shell of revolution with most coordinate systems. This difficulty is easily overcome by reverting to the global Cartesian coordinates of Ref. 8 at such a point, since any element in that region will also be shallow with respect to the latter coordinates. That is, the present rotation matrices $[R_1]$ and $[R_2^{-1}]$ are merely replaced by $[R_1]$ and $[R_2]$ given in Table 1 of Ref. 8 for a pole node.

3.2 Shell Curvatures

The shell element curvatures may be determined locally by specifying the shell elevations above the ξ,η base plane at the mid-side nodes 4, 5, 6 (Fig. 1) and using them in the quadratic function, equation (5) of Ref. 8. Note that the elevations are zero at the corner nodes 1, 2, 3. The locations of the mid-side nodes are determined first in the shell coordinates simply as averages of the corner node coordinates. The global coordinates of these nodes are then easily obtained from equations (8) and are substituted into equations (12) to yield the three elevations ζ_i and the corresponding base plane coordinates ξ_i, η_i for i = 4,5,6.

TABLE 1: TRANSFORMATION MATRIX [R]

$$[R] = \begin{bmatrix} [R_1]_1 & 0 & 0 & 0 & 0 & 0 & 0 \\ 0 & [R_2^{-1}]_1 & 0 & 0 & 0 & 0 & 0 \\ 0 & 0 & [R_1]_2 & 0 & 0 & 0 & 0 \\ 0 & 0 & 0 & [R_2^{-1}]_2 & 0 & 0 & 0 \\ 0 & 0 & 0 & 0 & [R_1]_3 & 0 & 0 \\ 0 & 0 & 0 & 0 & 0 & [R_2^{-1}]_3 & 0 \\ 0 & 0 & 0 & 0 & 0 & 0 & [R_3]_c \end{bmatrix}$$

where

$$[R_2] = \begin{bmatrix} 1 & 0 & 0 & 0 & 0 & 0 \\ 0 & \xi_\alpha & \eta_\alpha & 0 & 0 & 0 \\ \theta & \xi_\beta & \eta_\beta & 0 & 0 & 0 \\ 0 & \xi_{\alpha\alpha} & \eta_{\alpha\alpha} & \xi_\alpha^2 & 2\xi_\alpha\eta_\alpha & \eta_\alpha^2 \\ 0 & \xi_{\alpha\beta} & \eta_{\alpha\beta} & \xi_\alpha\xi_\beta & \xi_\alpha\eta_\beta+\xi_\beta\eta_\alpha & \eta_\alpha\eta_\beta \\ 0 & \xi_{\beta\beta} & \eta_{\beta\beta} & \xi_\beta^2 & 2\xi_\beta\eta_\beta & \eta_\beta^2 \end{bmatrix}$$

$$[R_3] = \begin{bmatrix} \xi_\alpha/a & \xi_\beta/b \\ \eta_\alpha/a & \eta_\beta/b \end{bmatrix} \qquad a = \sqrt{\xi_\alpha^2 + \eta_\alpha^2} \qquad b = \sqrt{\xi_\beta^2 + \eta_\beta^2}$$

$J = \xi_\alpha\eta_\beta - \xi_\beta\eta_\alpha$, $\xi_\alpha = \partial\xi/\partial\alpha$, etc.

Subscripts $[\ ]_i$ mean evaluated at node i or centroid c.

Table 1 (cont'd)

$$[R_1] = \begin{bmatrix} \xi_\alpha/a & 0 & 0 \\ \eta_\alpha^2(\xi_{\alpha\alpha}\eta_\beta - \xi_{\alpha\beta}\eta_\alpha)/Ja^3 + \xi_\alpha\eta_\alpha(\eta_\alpha\eta_{\alpha\beta} - \eta_\beta\eta_{\alpha\alpha})/Ja^3 & \xi_\alpha\eta_\beta/Ja & -\xi_\alpha\eta_\alpha/Ja \\ \eta_\alpha^2(\xi_\alpha\xi_{\alpha\beta} - \xi_\beta\xi_{\alpha\alpha})/Ja^3 + \xi_\alpha\eta_\alpha(\xi_\beta\eta_{\alpha\alpha} - \xi_\alpha\eta_{\alpha\beta})/Ja^3 & -\xi_\alpha\xi_\beta/Ja & \xi_\alpha^2/Ja \\ \eta_\alpha/a & 0 & 0 \\ \xi_\alpha^2(\eta_\beta\eta_{\alpha\alpha} - \eta_\alpha\eta_{\alpha\beta})/Ja^3 + \xi_\alpha\eta_\alpha(\xi_{\alpha\beta}\eta_\alpha - \xi_{\alpha\alpha}\eta_\beta)/Ja^3 & \eta_\alpha\eta_\beta/Ja & -\eta_\alpha^2/Ja \\ \xi_\alpha^2(\xi_\alpha\eta_{\alpha\beta} - \xi_\beta\eta_{\alpha\alpha})/Ja^3 + \xi_\alpha\eta_\alpha(\xi_{\alpha\alpha}\xi_\beta - \xi_\alpha\xi_{\alpha\beta})/Ja^3 & -\xi_\beta\eta_\alpha/Ja & \xi_\alpha\eta_\alpha/Ja \end{bmatrix}$$

$$\begin{bmatrix} \xi_\beta/b & 0 & 0 \\ \eta_\beta^2(\xi_{\alpha\beta}\eta_\beta - \xi_{\beta\beta}\eta_\alpha)/Jb^3 + \xi_\beta\eta_\beta(\eta_\alpha\eta_{\beta\beta} - \eta_\beta\eta_{\alpha\beta})/Jb^3 & \xi_\beta\eta_\beta/Jb & -\xi_\beta\eta_\alpha/Jb \\ \eta_\beta^2(\xi_\alpha\xi_{\beta\beta} - \xi_\beta\xi_{\alpha\beta})/Jb^3 + \xi_\beta\eta_\beta(\xi_\beta\eta_{\alpha\beta} - \xi_\alpha\eta_{\beta\beta})/Jb^3 & -\xi_\beta^2/Jb & \xi_\alpha\xi_\beta/Jb \\ \eta_\beta/b & 0 & 0 \\ \xi_\beta^2(\eta_\beta\eta_{\alpha\beta} - \eta_\alpha\eta_{\beta\beta})/Jb^3 + \xi_\beta\eta_\beta(\xi_{\beta\beta}\eta_\alpha - \xi_{\alpha\beta}\eta_\beta)/Jb^3 & \eta_\beta^2/Jb & -\eta_\alpha\eta_\beta/Jb \\ \xi_\beta^2(\xi_\alpha\eta_{\beta\beta} - \xi_\beta\eta_{\alpha\beta})/Jb^3 + \xi_\beta\eta_\beta(\xi_\beta\xi_{\alpha\beta} - \xi_\alpha\xi_{\beta\beta})/Jb^3 & -\xi_\beta\eta_\beta/Jb & \xi_\alpha\eta_\beta/Jb \end{bmatrix}$$

Note that these points do not necessarily coincide with the mid-side points of the base plane triangle. These results, together with the zero elevations at the three corner nodes, are then sufficient to complete the quadratic fit to the shell shape and determine the 6 coefficients. Finally, the three shell curvatures required in the strain energy calculation are obtained simply by differentiation.

Alternately, the shell curvatures for each element may be specified externally. This is the approach used for the results presented herein, since all example applications have constant curvatures anyway.

4.0 RESULTS

Both elements have been extensively tested [10,19] and only selected results are given below to emphasize the major characteristics of the two approaches and illustrate their effectiveness.

4.1 Rigid Body Modes

Rigid body modes have been calculated for a typical spherical shell element. The angular coordinates of the element analyzed are given at the top of Table 2, Poisson's ratio was taken as $\nu = 0.3$, $Et/(1-\nu^2)$ was set equal to 1 and R/t was fixed at 50. Three different sizes of element were analyzed, with R = 1,10 and 100. The first eight eigenvalues obtained using TSS and CURSHL (K-S) (Koiter-Sanders shell theory) are given in Table 2. Note that the first 'non-rigid' body mode, the seventh eigenvalue, has the same predicted value for all sizes of element for the two approaches. It is always substantially larger than the last 'rigid' body mode.

For TSS, λ_7 is always some seven orders of magnitude larger than λ_6, indicating that the first six eigenvalues are indeed rigid body modes. This is not surprising, since zero strain modes are polynomials in Donnell-Vlasov (D-V) or in shallow shell theory and these are represented exactly in TSS. The negative eigenvalues are extremely small and are probably due to round-off error.

For CURSHL (K-S), a smaller separation between λ_7 and λ_6 occurs, and this separation varies with the element size. This is expected, since zero strain modes are not exactly represented by polynomials in Koiter-Sanders shell theory and since an approximate numerical integration scheme is used. However, CURSHL (K-S) still gives excellent numerical results.

4.2 Uniformly Pressurized Sphere

This is a membrane type problem, with R/t = 50 and $\nu = 0.3$ (Fig. 2). Because of symmetry, only a wedge of the shell extending between the equator and the pole had to be analyzed. A uniformly spaced gridwork was used and results were obtained for N = 2,4,8 and 16. Typical non-dimensionalized strain energy, displacements

Finite Element Co-ordinates, Radians

i	1	2	3
α_i	0	0.174533	0
β_i	1.57080	1.74533	1.74533

Eigenvalues In Ascending Magnitude CURSHL (K-S)

No.	R = 1 t = 0.02	R = 10 t = 0.2	R = 100 t = 2
1	$.861 \times 10^{-14}$	$.206 \times 10^{-15}$	$.208 \times 10^{-17}$
2	$.765 \times 10^{-13}$	$.839 \times 10^{-15}$	$.838 \times 10^{-17}$
3	$.348 \times 10^{-12}$	$.655 \times 10^{-14}$	$.659 \times 10^{-16}$
4	$.462 \times 10^{-11}$	$.693 \times 10^{-13}$	$.697 \times 10^{-15}$
5	$.282 \times 10^{-10}$	$.504 \times 10^{-11}$	$.690 \times 10^{-13}$
6	$.969 \times 10^{-10}$	$.148 \times 10^{-10}$	$.203 \times 10^{-12}$
7	$.488 \times 10^{-8}$	$.487 \times 10^{-8}$	$.487 \times 10^{-8}$
8	$.731 \times 10^{-8}$	$.724 \times 10^{-8}$	$.720 \times 10^{-8}$
$\frac{\lambda_6}{\lambda_7}$	1.98×10^{-2}	3.02×10^{-3}	4.15×10^{-5}

Eigenvalues In Ascending Magnitude - TSS

No.	R = 1 t = 0.02	R = 10 t = 0.2	R = 100 t = 2
1	$-.736 \times 10^{-18}$	$.580 \times 10^{-18}$	$-.386 \times 10^{-18}$
2	$-.768 \times 10^{-18}$	$.676 \times 10^{-18}$	$.409 \times 10^{-18}$
3	$-.324 \times 10^{-17}$	$.167 \times 10^{-17}$	$-.139 \times 10^{-17}$
4	$.226 \times 10^{-16}$	$.209 \times 10^{-16}$	$.300 \times 10^{-16}$
5	$-.735 \times 10^{-15}$	$-.166 \times 10^{-15}$	$-.165 \times 10^{-14}$
6	$.121 \times 10^{-14}$	$.267 \times 10^{-14}$	$.245 \times 10^{-14}$
7	$.493 \times 10^{-8}$	$.493 \times 10^{-8}$	$.493 \times 10^{-8}$
8	$.747 \times 10^{-8}$	$.747 \times 10^{-8}$	$.747 \times 10^{-8}$
$\frac{\lambda_6}{\lambda_7}$	2.45×10^{-7}	5.41×10^{-7}	4.98×10^{-7}

Table 2. Rigid Body Modes for a Spherical Shell Segment Using Exact Curvatures: $\nu = 0.3$, $Et/(1-\nu^2)=1$, $R/t=50$

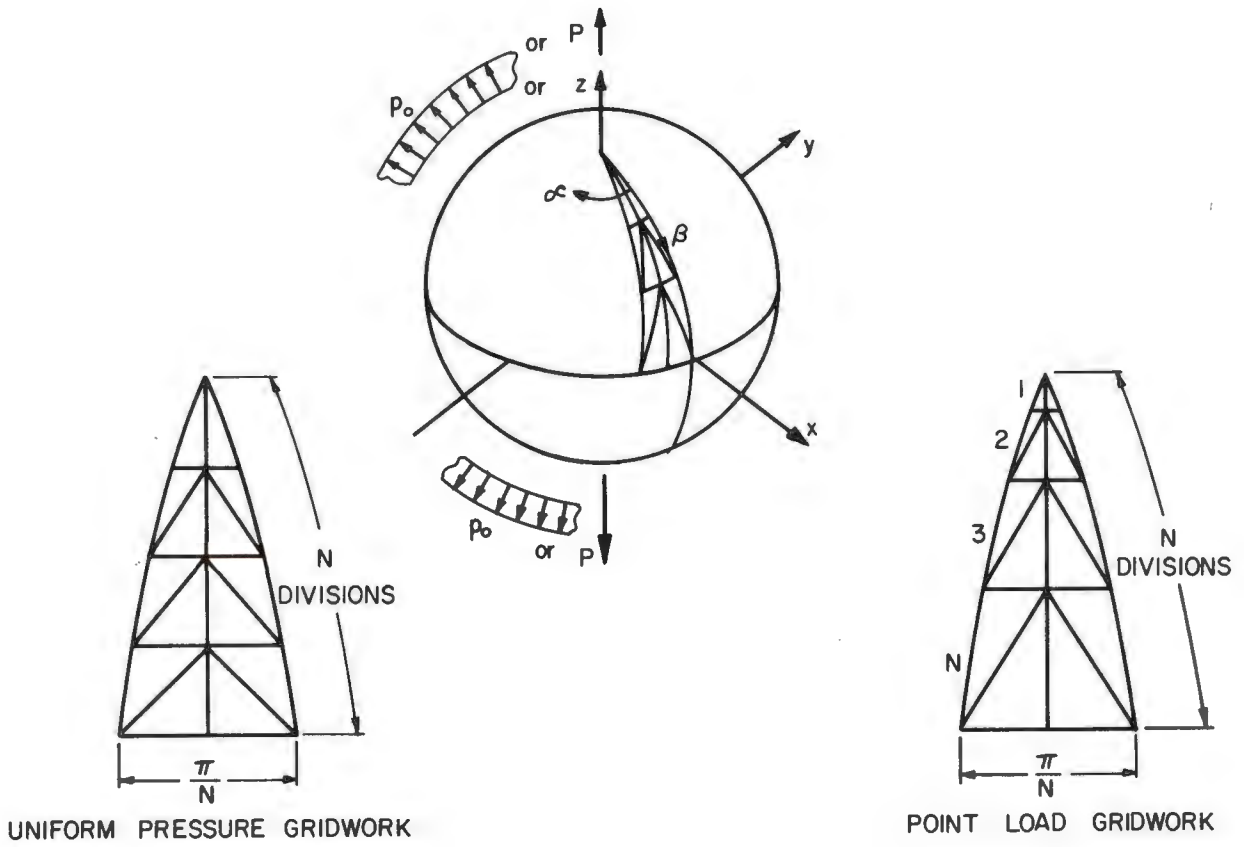

Figure 2. Spherical Shell Program
R/t = 50, ν = 0.3

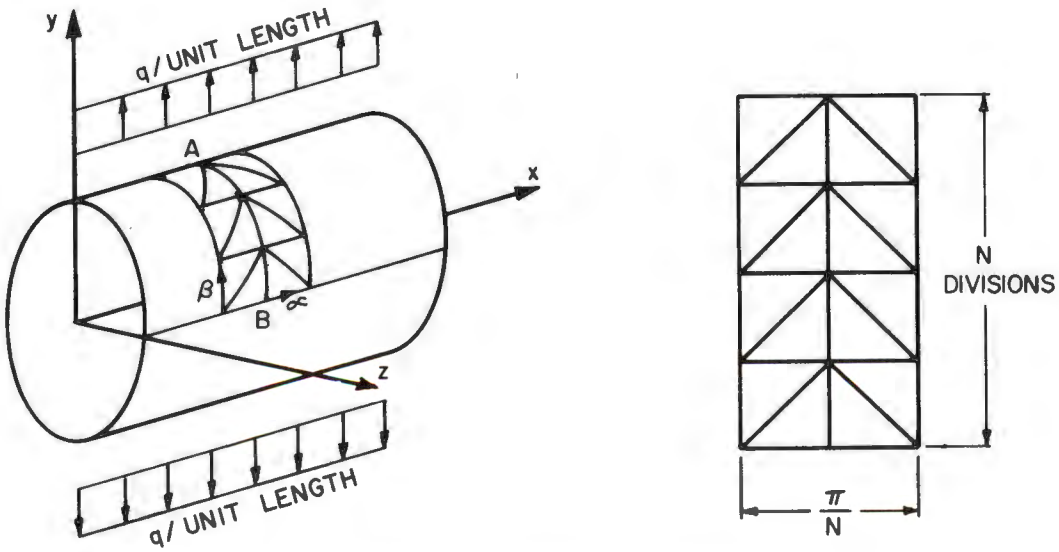

Figure 3. Infinitely Long Pinched Cylindrical Shell
R/t = 10, ν = 0.3

and stress resultants are given in Table 3.

The exact solution is a uniform radial outward displacement. Although the shape functions of both CURSHL and TSS can exactly represent this displacement, neither element quite achieves an exact solution. In the case of CURSHL, this is due to the approximate integration scheme used. The errors are extremely small however. TSS also gives excellent results and the strain energy convergence rate is slightly better than N^{-2}. Exact results are not obtained because TSS produces only an approximately conforming assemblage of elements.

4.3 Pinched Spherical Shell

The pinched sphere is a difficult problem in that there are regions of large bending stresses, regions where membrane action predominates and a region of high stress concentration. Regrettably, the problem is axi-symmetric but the authors have been unable to find a meaningful non-axi-symmetric problem for which a reasonable 'exact' solution exists. Again $R/t = 50$ and $\nu = 0.3$ were used and only a wedge of the shell was analyzed. A non-uniform gridwork spacing was used where the ratios of the sides of successive elements were taken as 1:2:3:4 .....N (Fig. 2). Two solutions were found using CURSHL, one with Koiter-Sanders (K-S) and one with Donnell-Vlasov (D-V) shell theory. These results together with the TSS results are given in non-dimensional form in Table 4 and Figures 4 to 9.

The displacement under the load (proportional to strain energy) is given in Table 4 and is plotted in Figure 4. All three results converge very rapidly, with CURSHL (K-S) converging to the 'asymptotic' solution given by Koiter [20]. Both TSS and CURSHL (D-V) are converging to a common result, some 0.5 percent below the Koiter solution, as a result of differences in shell theories. TSS slightly overshoots the solution for small values of N, not surprising since it is not fully conforming. The convergence rate of CURSHL (K-S) is close to N^{-4}. This is more rapid than that found for most point load problems [6,7,8] and probably occurs because of the non-uniform spacing of the gridworks. Table 4 also gives values for displacements and stresses at various points in the shell, and convergence of all these results is very rapid. Again, CURSHL (K-S) converges to different values than the other two results.

Displacement distributions near the load are given in Figure 5 for N = 5 and 10. These are compared to a shallow shell theory solution from Timoshenko [21], since it is extremely difficult to calculate distributions from the Koiter 'asymptotic' solution. Clearly, the Timoshenko solution is not precise enough, since it is approximately three percent lower than the Koiter solution under the load. The finite element solutions follow the shape of the Timoshenko solution closely but lie slightly above as expected. For N = 10, TSS and CURSHL (K-S) are indistinguishable, while for N = 5, minor differences are observed. CURSHL (D-V) has not been

	Deflection At Pole $\frac{Etw_p}{p_o R^2}$		Deflection at Equator $\frac{Etw_e}{p_o R^2}$		Stress Resultant At Pole $\frac{N_{\alpha p}}{p_o R} = \frac{N_{\beta p}}{p_o R}$	
N	CURSHL(K-S)	TSS	CURSHL(K-S)	TSS	CURSHL(K-S)	TSS
2	.350003	.3505	.349972	.3205	.50006	.4773
4	.350001	.3522	.350000	.3435	.50001	.4862
8	.350000	.3520	.350000	.3484	.50000	.4955
16		.3507		.3496		.4988
Exact	0.350000		0.350000		0.50000	

	Stress Resultants At Equator $N_{\alpha e}/p_o R$		$N_{\beta e}/p_o R$		Strain Energy $EtU/p_o^2 R^4$	
N	CURSHL(K-S)	TSS	CURSHL(K-S)	TSS	CURSHL(K-S)	TSS
2	.50006	.5291	.50001	.4884	2.65561544	2.3458
4	.50000	.4975	.50000	.5026	2.65561517	2.5724
8	.50000	.4989	.50000	.5011	2.65561511	2.6344
16		.4997		.5003		2.6503
Exact	0.50000		0.50000		2.65561509	

Table 3. Convergence of Displacements and Stresses of Uniform Pressure Loaded Spherical Shell: $R/t = 50$, $\nu = 0.3$

	Deflection Under Load $Et w_p/P$			Stress Resultant Under Load $RN_{\alpha p}/P = RN_{\beta p}/P$		
N	CURSHL(K-S)	CURSHL(D-V)	TSS	CURSHL(K-S)	CURSHL(D-V)	TSS
2	12.790	12.727	18.100	1.649	1.681	7.047
4	20.673	20.567	20.946	7.853	8.002	8.645
6	21.085	20.979	21.109	9.341	9.565	9.762
8	21.162	21.056	21.113	9.716	9.994	10.069
10	21.184	21.078	21.109	9.839	10.161	10.195
15	21.197	21.091	21.102	9.883	10.286	10.294
20	21.199	21.093	21.100	9.853	10.313	10.32
Koiter	21.2004					
Timoshenko	20.654					

	Deflection At Equator $Et w_e/P$			Stress Resultant At Equator $RN_{\beta p}/P$		
N	CURSHL(K-S)	CURSHL(D-V)	TSS	CURSHL(K-S)	CURSHL(D-V)	TSS
2	-.2994	-.2993	-.0867	.0611	.0615	.3071
4	-.2084	-.2083	-.2256	.1628	.1627	.1873
6	-.2069	-.2072	-.2161	.1602	.1602	.1686
8	-.2069	-.2068	-.2114	.1596	.1596	.1636
10	-.2069	-.2068	-.2094	.1594	.1593	.1617
15	-.2069	-.2068	-.2079	.1592	.1592	.1602
20	-.2069	-.2068	-.2069	.1591	.1591	.1597
Membrane	-0.2069			0.1592		

Table 4. Convergence of Displacements and Stresses of Point Loaded Spherical Shell; R/t = 50, ν=0.3

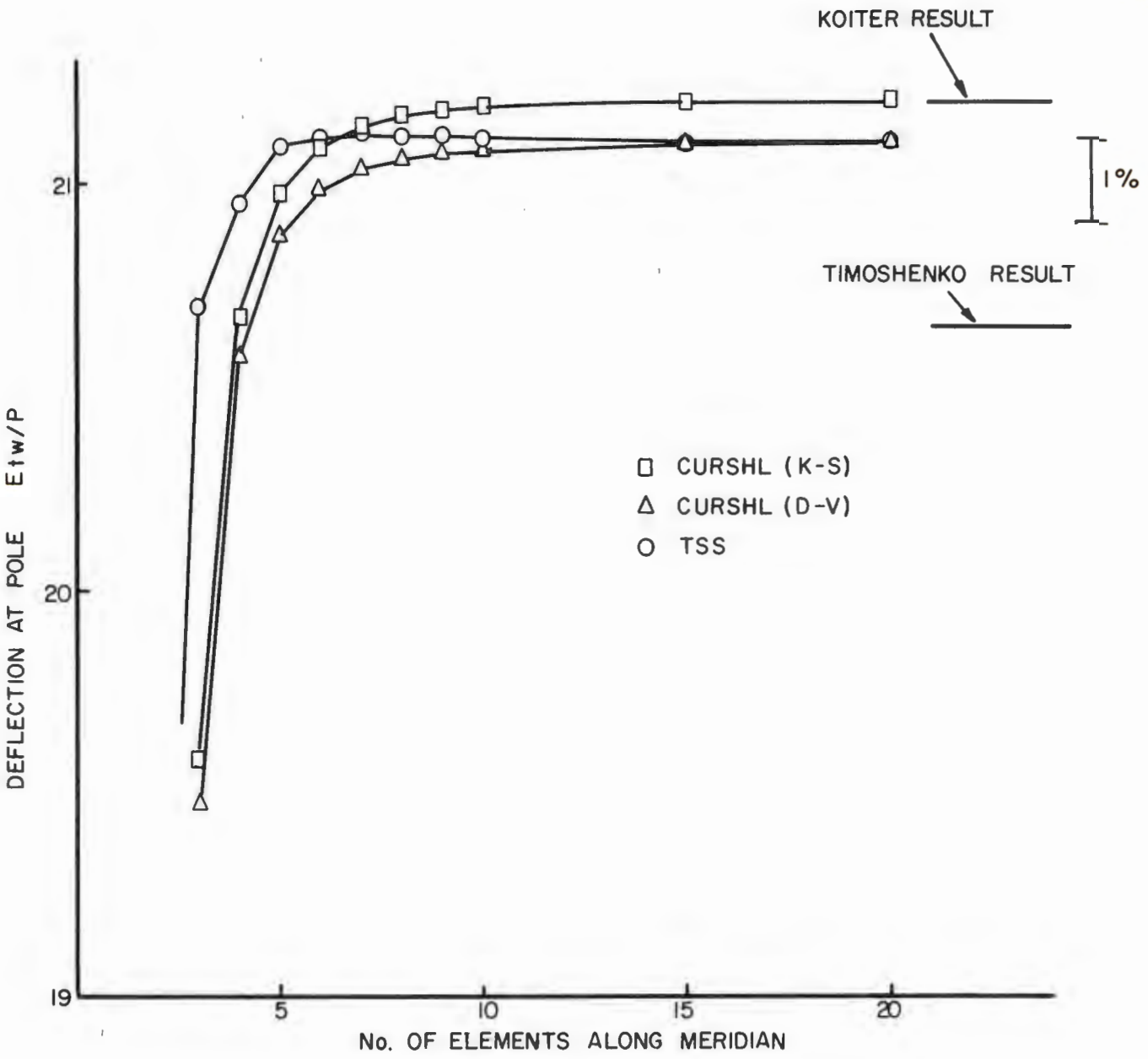

Figure 4. Displacement Under Point Load on Spherical Shell
R/t = 50, ν = 0.3

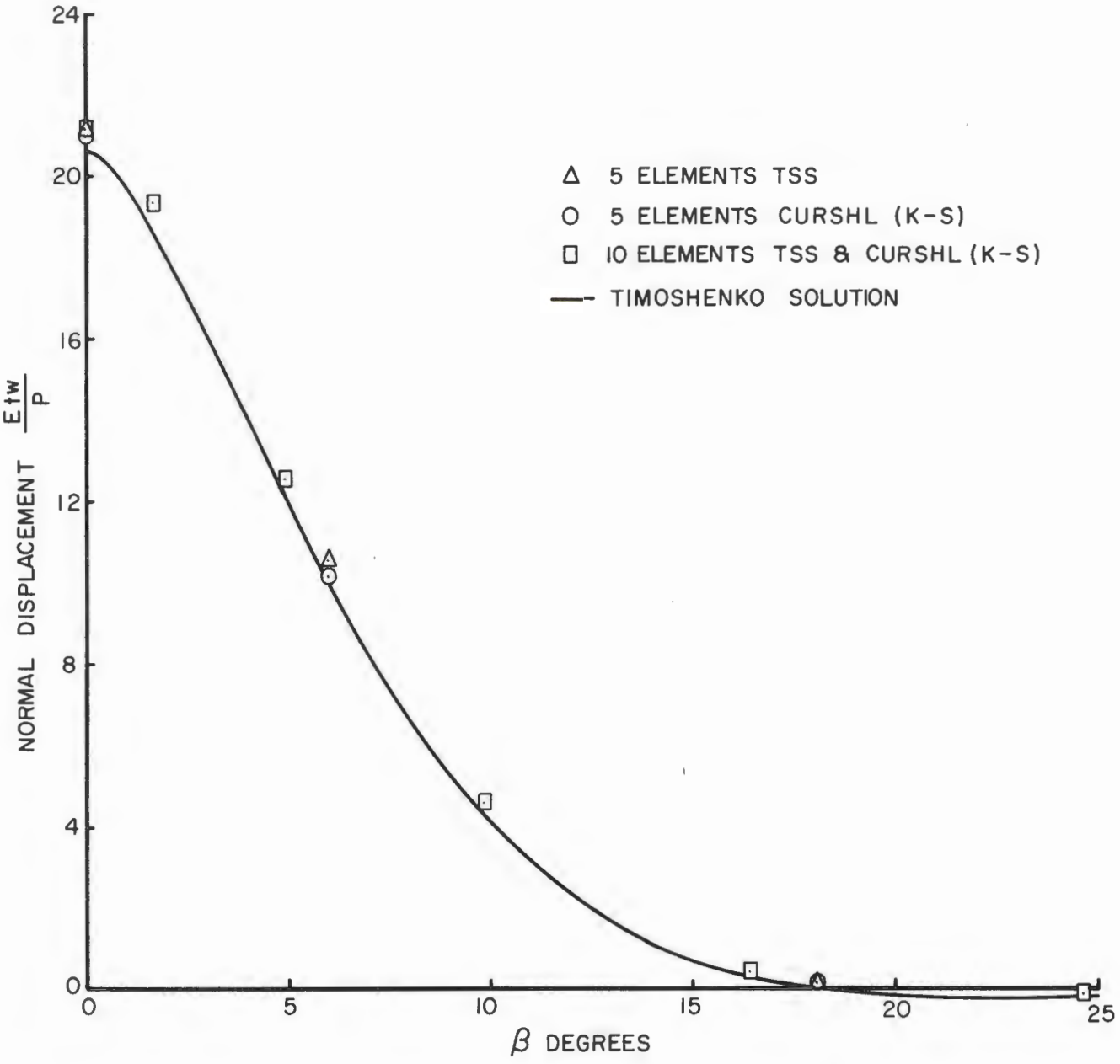

Figure 5. Displacement Near Pole of Point Loaded Sphere
R/t = 50, ν = 0.3

plotted since it is essentially identical with TSS.

The displacements are compared with the membrane solution well away from the load in Figure 6. For N = 10, both TSS and CURSHL (K-S) give 'exact' distributions, while for N = 5, there are slight differences. It appears that the membrane solution is valid for values of β greater than 40°. It is remarkable that the finite element results are so accurate well away from the load, since the displacements are over one order of magnitude smaller than the displacement under the load.

Bending stress and stress resultant distributions near the point load are given in Figures 7 and 8 for N = 5 and 10, and are compared with a Flügge 'asymptotic' solution [22]. These stresses are very accurately predicted by both methods and the only differences between TSS and CURSHL (K-S) occur near the point load.

Away from the point load, bending stresses die out and stress resultants may be compared with a membrane solution. This is done in Figure 9, where it may be seen that CURSHL (K-S) gives excellent results. TSS results lie close to the membrane solution for N_β but are still not quite converged for N_α. It must be remembered, however, that these stresses are much smaller than the critical stresses near the point load.

4.4 Infinitely Long Pinched Cylindrical Shell

This problem is a sensitive indicator of differences in shell theory. A Poisson's ratio of $\nu = 0.0$ was used and all x-direction degrees of freedom were constrained to be zero so that only a strip of the shell had to be analyzed (Fig. 3). An R/t ratio of 10 was chosen so that the strain energy of stretching would not be too small relative to the strain energy of bending. Uniform gridworks were used for a quarter of the cylinder and solutions have been obtained for N = 1,2,4,8 and 16.

The non-dimensional results obtained with CURSHL (K-S), CURSHL (D-V) and TSS are given in Table 5 together with exact results. All three results converge rapidly to the exact solutions, although the performance of CURSHL is significantly better than that of TSS. A plot of strain energy (directly proportional to displacement under the load) reveals that CURSHL is converging at a rate close to its predicted asymptotic value, N^{-6}, while TSS is converging at a rate of only N^{-2}. TSS converges to the Donnell-Vlasov theory results. This is not surprising since the shallow shell elements used in the transformation process are based on Donnell-Vlasov type equations for bending strains.

4.5 Timing Considerations

Computer timings and cost analyses are exceedingly difficult to present in a useful manner. Both elements have been programmed on IBM 360/67 computers, but different operating systems were used. Therefore, times given are not directly comparable. Double

	Deflection Under Line Load Etw_A/qR			Deflection 90° From Line Load Etw_B/qR		
	CURSHL(K-S)	CURSHL(D-V)	T.S.S.	CURSHL(K-S)	CURSHL(D-V)	T.S.S.
1	43.8757	33.1989	26.5908	-36.7181	-26.7111	-21.7275
2	86.9064	50.9793	47.1083	-79.3085	-44.1400	-40.7192
4	89.5872	51.9687	50.9115	-81.6603	-44.8811	-43.9443
8	89.6583	51.9949	51.7278	-81.7207	-44.8989	-44.6623
16	-	-	51.9286	-	-	-44.8400
Exact K-S	89.6597			-81.7219		
Exact D-V		51.9954			-44.8992	

	Stress Resultant Under Line Load N_A/q			Bending Moment Under Line Load M_A/qR		
	CURSHL(K-S)	CURSHL(D-V)	T.S.S.	CURSHL(K-S)	CURSHL(D-V)	T.S.S.
1	-7.675	-5.6685	4.2566	.23044	.21347	.09713
2	-3.338	-1.969	2.2108	.31616	.26077	.21582
4	-0.533	-0.0853	0.9945	.31839	.26181	.24997
8	-0.067	0.2616	0.5244	.31832	.26180	.25875
16	-	-	0.3751	-	-	.26103
Exact K-S	0.0			+0.31831		
Exact D-V		0.3183			+0.26180	

Table 5. Convergence of Displacements and Stresses of Infinitely Long Pinched Cylindrical Shell: $R/t = 10$, $\nu = 0.0$.

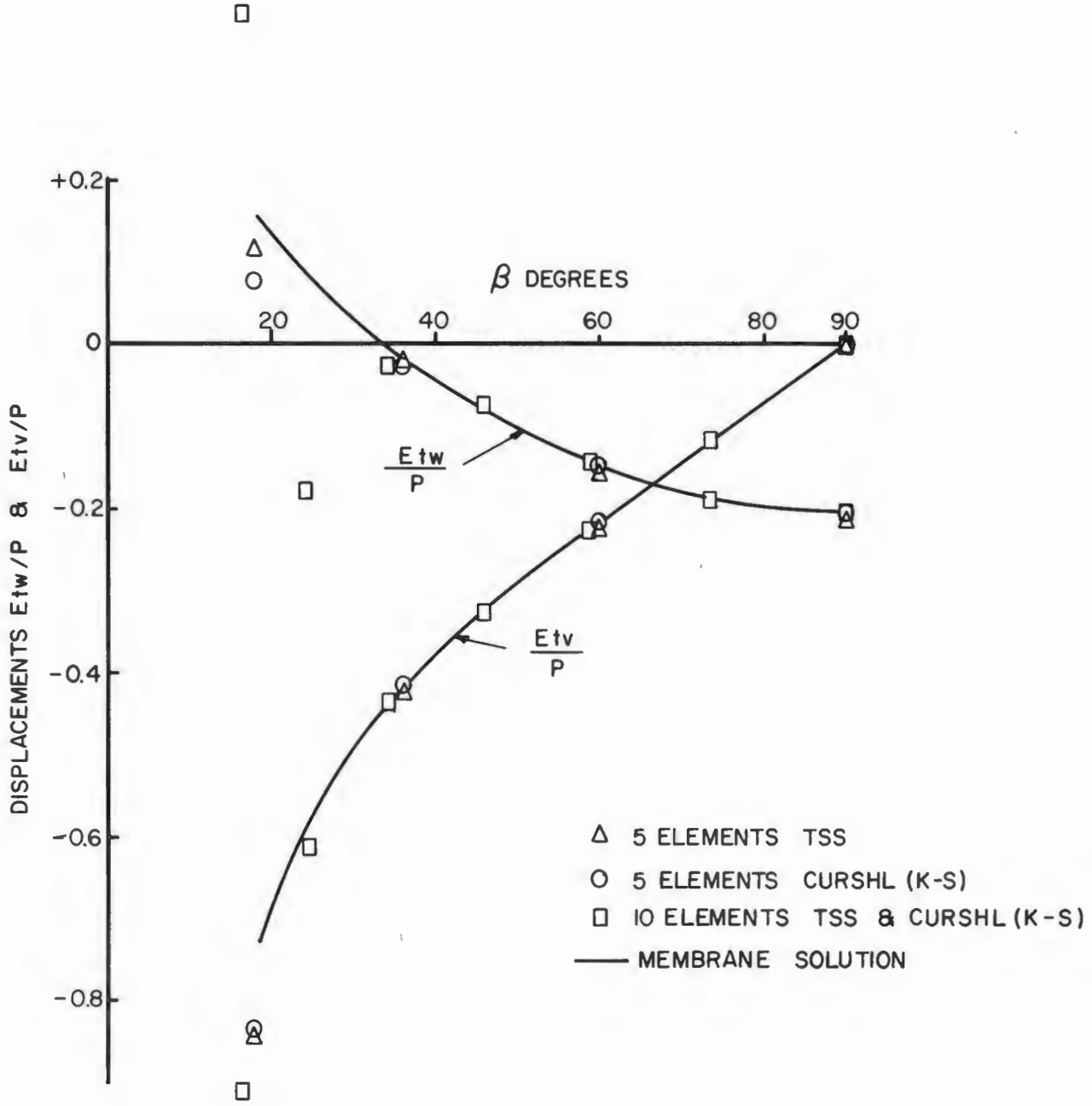

Figure 6. Displacements Remote From Pole of Point Loaded Sphere
R/t = 50, ν = 0.3

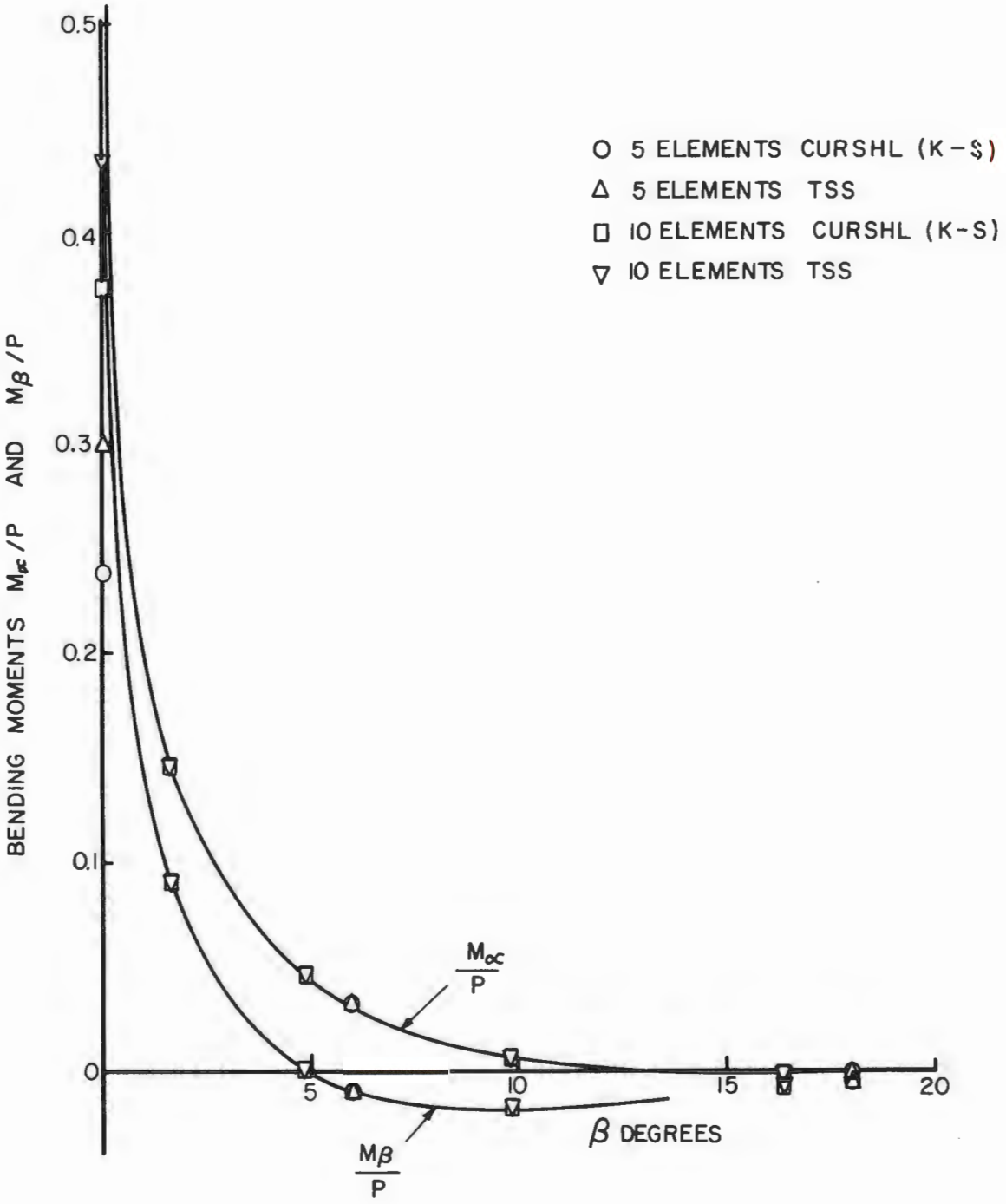

Figure 7. Moments Near Pole of Point Loaded Sphere
R/t = 50, ν = 0.3

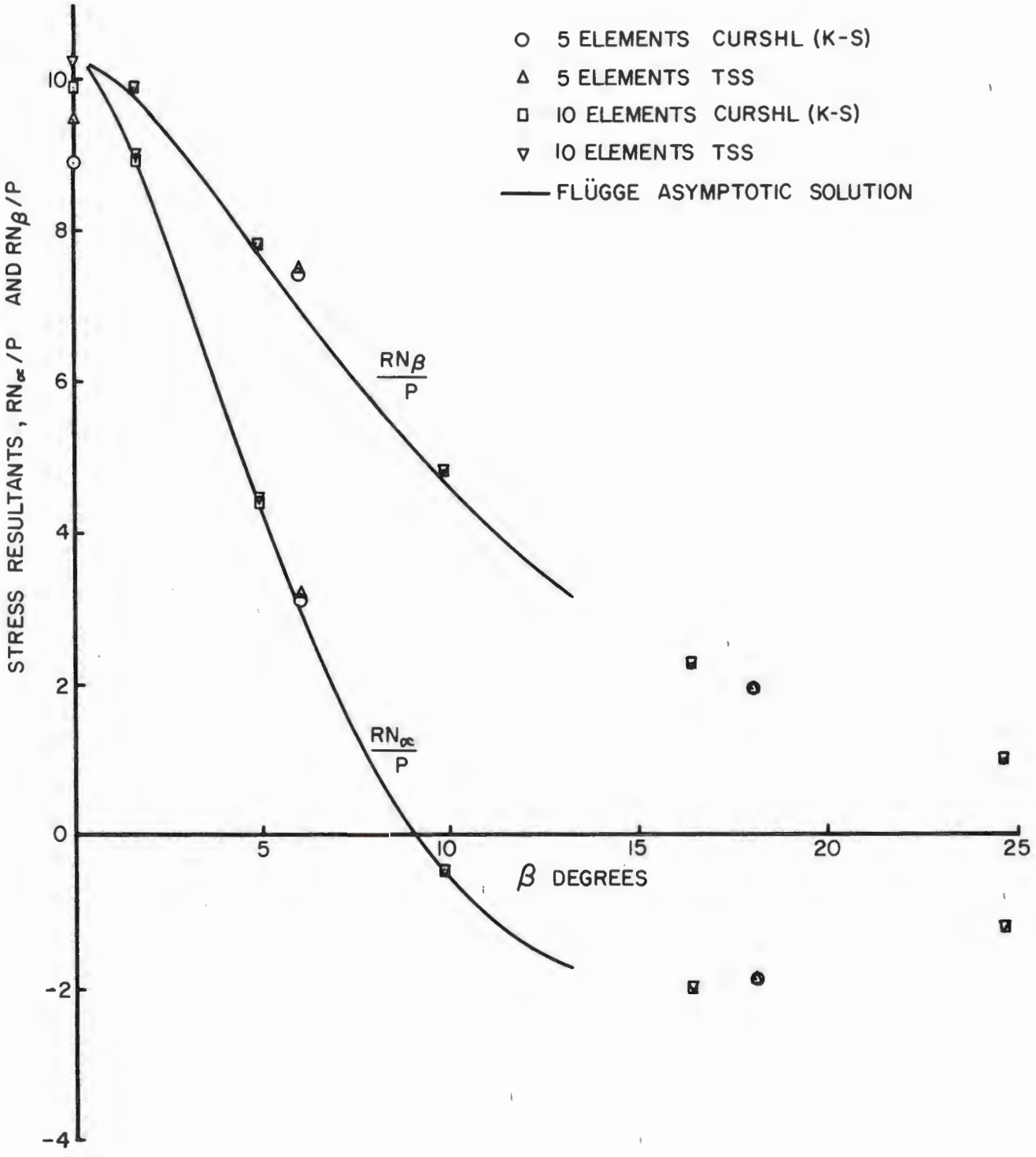

Figure 8. Stress Resultants Near Pole of Point Loaded Sphere
R/t = 50, ν = 0.3

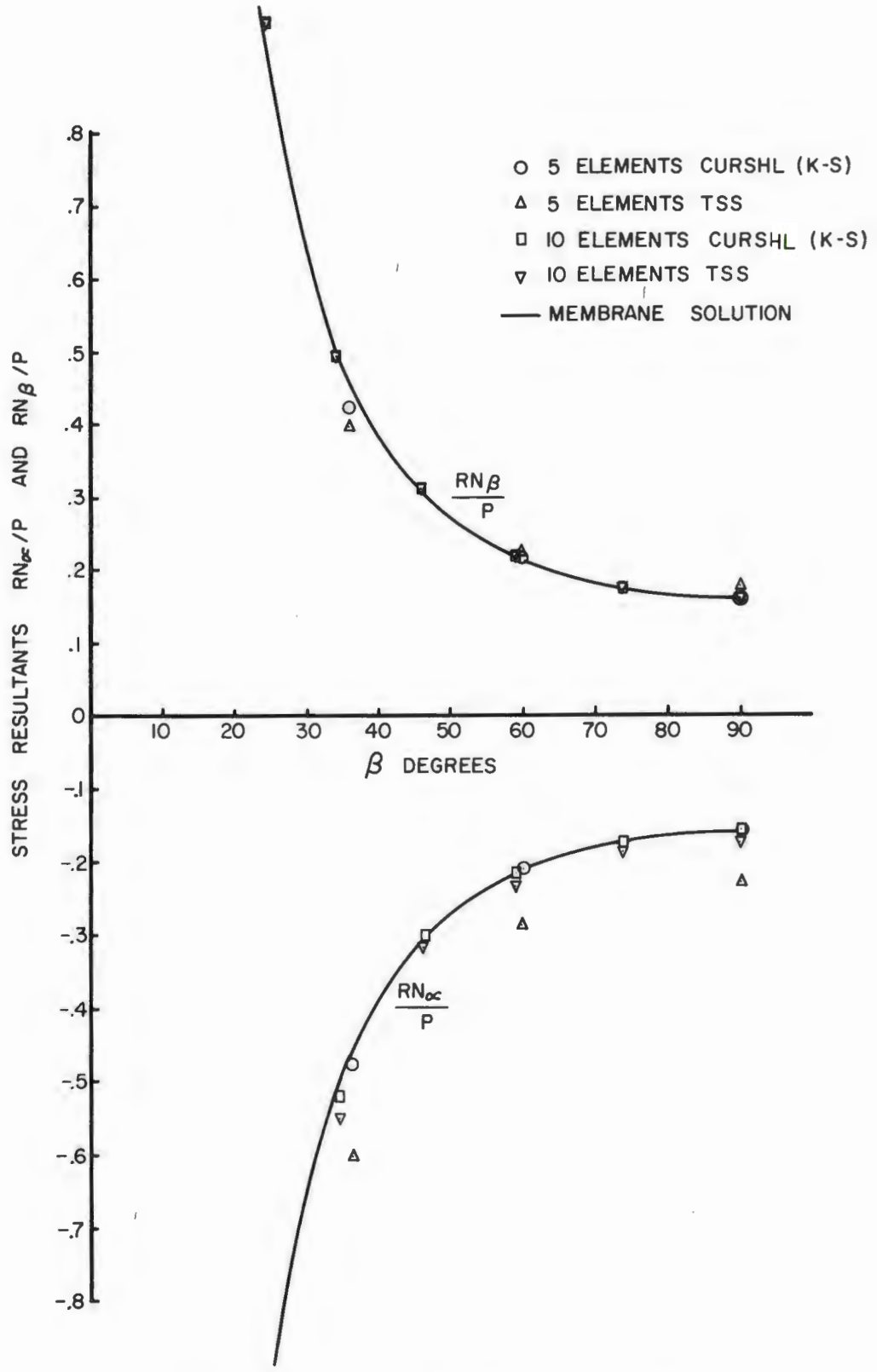

Figure 9. Stress Resultants Remote From Pole of Point Loaded Sphere: $R/t = 50$, $\nu = 0.3$

precision arithmetic was used throughout.

CURSHL has been run on the IBM System/360 Time Sharing System using full H level Fortran. CURSHL (K-S) takes approximately 1.6 seconds of VMR time to generate stiffness matrix, while CURSHL (D-V) takes only 1.3 seconds. It must be remembered that an approximate integration scheme has been used; times would be increased if a more precise integration scheme were desired.

TSS has been run on the Michigan Terminal System (MTS) and only part of the program is in H level Fortran. TSS takes approximately 1.5 seconds of CPU time to generate one stiffness matrix. This includes an exact, closed form generation of the shallow shell stiffness matrix involved. Equation solving times are exactly the same since the same degrees of freedom are used in both approaches.

4.6 Comparison with other Elements

Space precludes extensive comparison of TSS, CURSHL and other elements. As well, writers seldom agree on the choice of test problems, making direct comparisons difficult. However, mention must be made of several other elements. Argyris and Scharpf [12] have developed SHEBA, a general triangular shell element that uses complete fifth order polynomials for u, v and w. This leads to an excessive, 18 degrees of freedom per node (see Section 2) and results using this element should be very similar to TSS or CURSHL at the expense of much greater computational effort. Key [3] has developed SLADE, a shell code based on a quadrilateral shell element which includes shear deformation. The element has nine degrees of freedom per node and is restricted to shells of revolution. SLADE gives good results but comparisons [10,19] indicate that the present approaches are superior. In addition, there are no shape limitations.

A third approach is that of Ahmad et al [23] who generate three-dimensional isoparametric finite elements into shell elements by restricting the variation of displacements through the thickness of each element. While valid for quite thick shells, their elements do not appear to compete with CURSHL or TSS for thin shells. Several other shell elements have been developed and are discussed at greater length in Ref. 10 and 19.

5.0 CONCLUSIONS

Two approaches to the finite element solution of arbitrary deep shells have been presented and compared. Both the arbitrary deep shell (CURSHL), and the transformed shallow shell (TSS) give excellent accuracy and both converge rapidly to the exact solutions as the number of elements used is increased. Good predictions of stress resultants and bending moments are obtained as well as of displacements. Engineering accuracy is always achieved with the use of a few elements.

CURSHL is a more flexible code with two general shell theories, Koiter-Sanders and Donnell-Vlasov, available as options, whereas TSS gives only Donnell-Vlasov theory solutions. While Donnell-Vlasov theory can be in error in special cases (as in Sec. 4.4), it is generally accepted that it is adequate for most practical shell problems where bending occurs in limited regions.

The predicted asymptotic rate of convergence for CURSHL of N^{-6} has been numerically confirmed and this rate is significantly greater than N^{-2}, the rate found for the non-conforming TSS approach. However, for a small number of elements, the accuracy of both methods is quite similar (though CURSHL generally gives better results). It has been demonstrated that the approximate numerical integration used in CURSHL is adequate and it is not necessary to explicitly include rigid body modes in an element. TSS is potentially the faster code, and it certainly is easier to program. With the verification of the validity and accuracy of these two approaches, perhaps the quest for 'a good, accurate, arbitrary triangular general shell finite element' may now be at an end.

REFERENCES

1. Gallagher, R., "Analysis of Plate and Shell Structures", Proc. of Symposium on Application of Finite Element Methods in Civil Engineering, Vanderbilt University, Nashville, Tennessee, Nov. 13-14, 1969.

2. Zienkiewicz, O.C., "The Finite Element Method: From Intuition to Generality", Applied Mechanics Reviews, Vol. 23, March 1970.

3. Key, S.W., "The Analysis of Thin Shells with a Doubly Curved Arbitrary Quadrilateral Finite Element", Paper presented at the Lockheed Conference on Computer Oriented Analysis of Shell Structures, Lockheed Palo Alto Research Lab., Palo Alto, Calif., Aug. 10-14, 1970.

4. Hartung, R.F., "An Assessment of Current Capability for Computer Analysis of Shell Structures", Air Force Flight Dynamics Lab., Air Force Systems Command, Wright Patterson Air Force Base, Dayton, Ohio, Technical Report AFFDL-TR-67-194, Preliminary Draft, Feb. 1970.

5. Lindberg, G.M., Olson, M.D., and Cowper, G.R., "New Developments in the Finite Element Analysis of Shells", National Research Council of Canada DME/NAE Quarterly Bulletin No. 1969(4).

6. Cowper, G.R., Kosko, E., Lindberg, G.M., and Olson, M.D., "A High Precision Triangular Plate-Bending Element", National Research Council of Canada, Aeronautical Report LR-514, Dec. 1968.

7. Cowper, G.R., Kosko, E., Lindberg, G.M., and Olson, M.D., "Static and Dynamic Applications of a High Precision Triangular Plate-Bending Element", AIAA Journal, Vol. 7, No. 10, pp. 1957-1965, 1969.

8. Cowper, G.R., Lindberg, G.M., and Olson, M.D., "A Shallow Shell Finite Element of Triangular Shape", Int. Journal of Solids and Structures, Vol. 6, pp. 1133-1156, 1970.

9. Lindberg, G.M., and Olson, M.D., "A High Precision Triangular Cylindrical Shell Finite Element", AIAA Journal, Vol. 9, No. 3, pp. 530-532, 1971.

10. Cowper, G.R., "CURSHL: A High-Precision Finite Element for Shells of Arbitrary Shape", National Research Council of Canada, Aeronautical Report, 1971 (in preparation).

11. McLay, R.W., "Completeness and Convergence Properties of Finite Element Displacement Functions: A General Treatment", AIAA Paper No. 67-143, AIAA 5th Aerospace Sciences Meeting, New York, Jan. 1967.

12. Argyris, J.H., and Scharpf, D.W., "The SHEBA Family of Shell Elements for the Matrix Displacement Method", Aeronautical Journal, Vol. 72, No. 694, pp. 873-883, 1968.

13. Greene, B.E., Jones, R.E., McLay, R.W., and Strome, D.R., "Dynamic Analysis of Shells Using Doubly-Curved Finite Elements", Proc. of the Second Conference on Matrix Methods in Structural Mechanics, AFFDL-TR-68-150, Wright-Patterson Air Force Base, October 1968.

14. Koiter, W.T., "A Consistent First Approximation in the General Theory of Elastic Shells", Proc. of IUTAM Symposium on the Theory of Thin Elastic Shells, Delft, 1959.

15. Budiansky, B., and Sanders, J.L., Jr., "On the 'Best' First-Order Linear Shell Theory", Progress in Applied Mechanics, (The Prager Anniversary Volume), The Macmillan Co., New York, 1963.

16. Novozhilov, V.V., "Thin Shell Theory", Sec. 17, P. Noordhoff Ltd., Gronigen, The Netherlands, 2nd Ed., 1964.

17. Green, A.E., and Zerna, W. "Theoretical Elasticity", Chapter XI, Oxford, Clarendon Press, 1954.

18. Ibid., Chapter I.

19. Olson, M.D., "Analysis of Arbitrary Shells Using Shallow Shell Finite Elements", Dept. of Civil Engineering Structural Research Series Report, University of British Columbia, 1971 (in preparation).

20. Koiter, W.T., "A Spherical Shell Under Point Loads at its Poles", Progress in Applied Mechanics (The Prager Anniversary Volume), Macmillan, New York, 1963.

21. Timoshenko, S.P., and Woinowsky-Krieger, S., "Theory of Plates and Shells", 2nd Ed., pp. 558-561, McGraw-Hill, New York, 1959.

22. Flügge, W., "Stresses in Shells", pp. 350-353, Springer-Verlag, Berlin/Gottingen/Heidelberg, 1960.

23. Ahmad, S., Irons, B.M. and Zienkiewicz, O.C., "Analysis of Thick and Thin Shell Structures by Curved Finite Elements", Int. J. for Num. Meth. in Eng., Vol. 2, No. 3, 1970, pp. 419-451.